

Effect of Zr Addition on the Corrosion of Ti in Acidic and Reactive Oxygen Species (ROS)-Containing Environments

Zhang, Y, Davenport, A, Burke, B, Addison, O & Vyas, N

Author post-print (accepted) deposited by Coventry University's Repository

Original citation & hyperlink:

Zhang, Y, Davenport, A, Burke, B, Addison, O & Vyas, N 2018, 'Effect of Zr Addition on the Corrosion of Ti in Acidic and Reactive Oxygen Species (ROS)-Containing Environments' *ACS Biomaterials Science and Engineering*, vol 4, no. 3, pp. 1103-1111
<https://dx.doi.org/10.1021/acsbiomaterials.7b00882>

DOI 10.1021/acsbiomaterials.7b00882

ESSN 2373-9878

Publisher: American Chemical Society

This document is the Accepted Manuscript version of a Published Work that appeared in final form in *ACS Biomaterials Science and Engineering*, copyright © American Chemical Society after peer review and technical editing by the publisher. To access the final edited and published work see <https://dx.doi.org/10.1021/acsbiomaterials.7b00882>

Copyright © and Moral Rights are retained by the author(s) and/ or other copyright owners. A copy can be downloaded for personal non-commercial research or study, without prior permission or charge. This item cannot be reproduced or quoted extensively from without first obtaining permission in writing from the copyright holder(s). The content must not be changed in any way or sold commercially in any format or medium without the formal permission of the copyright holders.

This document is the author's post-print version, incorporating any revisions agreed during the peer-review process. Some differences between the published version and this version may remain and you are advised to consult the published version if you wish to cite from it.

The effect of Zr addition on the corrosion of Ti in acidic and reactive oxygen species (ROS)-containing environments

Yue Zhang¹, Alison Davenport¹, Bernard Burke^{2,3}, Nina Vyas², Owen Addison^{2,4}*

¹ School of Metallurgy and Materials, University of Birmingham, Birmingham, B15 2TT, UK

² Biomaterials Unit, School of Dentistry, University of Birmingham, Birmingham, B5 7EG, UK

³ Faculty of Health & Life Sciences, Coventry University, Coventry, CV1 5LW, UK

⁴ School of Dentistry, University of Alberta, Edmonton, T6G 1C9, Canada

*corresponding author

Email: o.addison@bham.ac.uk; Tel: +44 (0)121 466 5506

KEYWORDS: titanium zirconium alloys, corrosion, HCl, H₂O₂, macrophages

ABSTRACT

The effect of systematic Zr additions on the corrosion behavior of Ti was studied in both acidic and Reactive Oxygen Species (ROS) containing environments, including macrophage cell culture, simulating inflammation associated with metallic implants. Electrochemical measurements on commercially-pure (CP) Ti, Zr and TiZr alloys showed that increasing Zr additions progressively enhanced Ti passivity in both acidic (HCl) and oxidative (H₂O₂) environments. However, a Ti50Zr alloy was found with increased pitting susceptibility. Corrosion was also evaluated using mass-spectrometry to determine metal ion release following

exposure of the alloys to THP-1 macrophage cell cultures, transformed into either their M1 (inflammatory states) or M2a (tissue repair states) phenotypes. The magnitude of ion release was reduced with increasing Zr contents, consistent with electrochemical observations. Nevertheless, optimized Zr content in Ti should balance both passivity and pitting resistance.

1 INTRODUCTION

Commercially pure titanium (CP Ti) is commonly used for dental implants owing to its biocompatibility and suitable mechanical strength.¹ However, there is increasing interest in the use of small diameter dental implants, which require alloys with higher mechanical strength to decrease the risk of fracture in service.² Newly-developed Ti alloys include a binary TiZr alloy (Roxolid®, Straumann) containing between 13%-18% Zr (exact composition undisclosed).² The TiZr-Roxolid® alloy shows enhanced mechanical strength with similar osseointegration properties and biocompatibility when compared with CP Ti.² The improvement in mechanical properties has been attributed to the solid solution strengthening mechanism.³⁻⁵ An experimental TiZr alloy with 50% (wt%) Zr has been shown to have a surface hardness and tensile strength increased by approximately 2.5 fold when compared with pure Ti or Zr.⁴

Exposure of Ti and Zr to air and to neutral solutions results in the spontaneous formation of a passive surface oxide layer which protects the underlying metal from further corrosion.⁶⁻⁸ The corrosion resistance of a number of discrete compositions of binary TiZr alloys has been previously reported in both standard testing solutions and in simulated physiological electrolytes.⁹⁻¹² Yu et al. showed an enhanced oxide film stability of Ti50Zr (wt%) when compared with that of CP Ti in de-aerated 5 M HCl solutions, and a reduced rate of dissolution at low potentials which could suggest enhanced corrosion resistance in crevice conditions.^{10, 11} Moreno et al. showed that Ti20Zr (wt%) passivates more rapidly and maintains a more stable passive surface than CP Ti in Ringer's solution across various pH (3.4, 7.6 and 8.9).⁹ It has been suggested that a Ti12Zr (wt%) alloy exhibits improved corrosion behaviour when compared with CP Ti and Ti6Al4V when tested in physiological solutions containing cultured human cells.¹² The corrosion behaviour of Ti alloys with additions of Zr between 5% and 20% (wt%) was

investigated with potentiodynamic sweeps, leading to the conclusion that Ti15Zr is more corrosion resistant than CP Ti in 0.9% NaCl solutions.¹³ Ti alloys with higher Zr additions (from 55% to 95% in wt%) showed higher passivity of Ti in fluoride-containing solutions,^{14, 15} but increased pitting corrosion in chloride-containing solutions.¹⁶

The corrosion behaviour of CP Ti depends upon its environment.^{17, 18} In a neutral environment such as extracellular fluid, Ti forms a highly corrosion-resistant passive film. However, metal implants with parts that are press-fit together, for example modular hip implants, mechanically-assisted crevice corrosion (MACC) can take place,^{19, 20} in which micromotion between the surfaces de-passivates the Ti leading to rapid corrosion forming titanium ions, which hydrolyse forming highly acidic solutions that favour continuing corrosion rather than re-passivation of the metal. Alternatively, the implant may be exposed to inflammatory biomolecules such as Reactive Oxygen Species (ROS), including H₂O₂, produced during tissue inflammation.²¹ Extensive studies have shown that H₂O₂ significantly enhances corrosion of Ti,^{17, 22-26} however, there seems no work has been conducted studying the effects of H₂O₂ (at physiological relevant levels) on the corrosion of TiZr or pure Zr. While studying the role of H₂O₂ in vitro can provide some insight into the underlying mechanisms affecting corrosion in the presence of ROS, it is desirable to complement such studies by investigating corrosion in cell cultures.²⁷⁻²⁹ Innate immune cells including macrophages can release ROS in response to pathogens and to foreign bodies, and have been shown to interact with Ti implant surfaces and modify corrosion resistance.^{21, 27, 28}

The aim of this study is to characterise the corrosion resistance of CP Ti, CP Zr and three binary TiZr alloys to investigate the effect of systematic Zr additions (0, 5, 15, 50 and 100 at%) on the corrosion of Ti in different electrolytes including an environment that represents local

acidification as a consequence of MACC (2 M HCl), one that represents an inflammatory environment (0.1 M H₂O₂), and an environment containing macrophages that are stimulated to generate more realistic ROS. Macrophage phenotypic diversity is better described as a spectrum rather than a set of distinct states; macrophage phenotypes are flexible, reversible and overlapping rather than fixed, final, and discrete. However broadly speaking, macrophage phenotypes can be classified as pro-inflammatory (M1) or anti inflammatory/wound healing (M2). The M2 state can be further subdivided into M2a, M2b, and M2c depending on the exact stimuli used to generate them.³⁰⁻³² M2 macrophages are generally considered to be low ROS producers, but are capable of ROS generation when exposed to the appropriate stimuli.³³

2 MATERIALS AND METHODS

2.1 Materials

Binary TiZr alloy rods (diameter 10 mm) with 5%, 15%, and 50% Zr (at%) were commercially sourced (American Elements®, USA). All grades were cast and melted at least three times to ensure homogeneity. CP Ti (Grade 2, Titanium Products Ltd, Solihull, UK) discs (diameter 10 mm and thickness 1 mm) and CP Zr (Grade 702, GoodFellow, UK) rod (diameter 10 mm) were obtained. The compositions of the five alloys are listed in Table 1.

Table 1. The composition (wt%) of TiZr binary alloys (Certificate of Analysis, American Elements[®]), CP Ti (Grade 2) and CP Zr (Grade 702) (manufacturer’s compositional certificates).

Alloys	Fe	Ni	Mg	Al	Si	Cu	Hf	Cr	C	O	N	H	Zr	Ti
CP Ti	0.03	-	-	-	-	-	-	-	0.01	0.13	<0.01	0.002	-	Bal.
Ti5Zr	0.075	0.002	0.002	0.018	0.005	0.016	-	-	< 0.01	< 0.08	-	-	9	Bal.
Ti15Zr	0.069	0.002	0.002	0.016	0.005	0.015	-	-	< 0.01	< 0.08	-	-	25	Bal.
Ti50Zr	0.048	0.002	0.003	0.012	0.007	0.009	-	-	< 0.01	< 0.08	-	-	66	Bal.
CP Zr	0.07	-	-	-	-	-	2.36	0.01	0.015	0.11	0.007	0.002	Bal.	-

2.2 Sample Preparation

The alloys were machined into 1 mm thickness discs for subsequent characterisation and testing. Samples for optical and electron microscopy were mounted, wet polished from 800 to 4000 grit using SiC abrasive papers and finished with OP-S colloidal silica suspension (0.04 μm) on MD-Chem cloth (Struers, Ballerup, Denmark) to obtain a consistent mirror surface finish. As-polished CP Ti, Ti5Zr and Ti15Zr samples were rinsed and sonicated with deionised water (Millipore, $>15 \text{ M}\Omega\text{cm}$), and methanol, followed by etching in Kroll's agent (2% HF, 6% HNO_3 and 92% H_2O). Ti-50Zr was etched separately in diluted Kroll's agent (0.5% HF, 5% HNO_3 , balanced with H_2O), prior to optical microscopy.

Samples for electrochemistry tests were cold-mounted in a non-conductive resin and polished to mirror surface finish using the previously described methods. The surfaces of prepared samples were rinsed with deionised water and 100% methanol and dried in an oil-free air stream. To ensure consistency in the surface oxide layer formed on different samples, each sample was exposed in ambient laboratory air for a fixed time of 15 mins following final surface polishing, prior to electrochemical characterisation.

Samples for immersion measurements in cell culture were prepared by wet polishing from 400, 800, 1200 to 2500 grit and finished with 4000 grit using endotoxin free water (sterile filtered, $<0.005 \text{ EU/mL}$, Sigma Aldrich, UK) as the lubricant. Polished discs were then sonicated with methanol and endotoxin free water for 10 mins, respectively, in sterilised glassware.

2.3 Electrochemical Measurements

Naturally-aerated 2 M HCl solutions were prepared from reagent grade HCl (30 wt% in H_2O , Fisher Scientific, UK) and diluted with deionised water. Physiological saline (0.15 M NaCl, 0.9 wt%) was prepared by dissolving NaCl (Sigma Aldrich, UK) in deionised water. H_2O_2

(30 wt% in H₂O, Sigma Aldrich, UK) was added in 0.9% NaCl solutions to give concentration of 0.1 M. The H₂O₂ stock solution was kept stored at 4±2 °C. A three-electrode cell was used for electrochemical tests, which was maintained at a temperature of 37±1 °C. The cold-mounted samples were used as working electrodes, Pt mesh was the counter electrode and a Saturated Calomel Electrodes (SCE) was the reference electrode. All the potentials are referenced to this scale.

Open Circuit Potentials (OCP) of samples were measured for 1 h allowing potentials to reach stable values (Gill AC potentiostat, ACM Instruments). Subsequently, anodic polarisation curves were then measured from -50 mV vs. OCP at a scan rate of 1 mV/s. Cathodic polarisation curves were measured from +50 mV vs. OCP at a scan rate of 1 mV/s. In addition, to study the effect of H₂O₂ on dissolution rate, potentiostatic polarisation was performed at 500 mV (vs. SCE) following 1 h immersion at OCP in 0.9% NaCl. At 1000 s of the potentiostatic tests, a solution of 0.9% NaCl containing H₂O₂ was added to give a final concentration of 0.1 M H₂O₂, which was stirred to ensure complete mixing. Control experiments were performed in parallel where the solution was stirred at the same time points without any addition of H₂O₂.

All electrochemical tests were repeated at least twice using newly prepared samples and solutions to confirm consistency of the measurements.

2.4 Corrosion (ion release) in macrophages cell culture

Metal discs were sterilised by incubating in 70% ethanol for 1 h followed by rinsing in endotoxin-free RPMI-1640 medium (R8758, Sigma Aldrich, UK). Sterilised discs were placed into 24 well plastic plates which had been pre-blocked with a 10% fetal bovine serum (FBS) supplemented RPMI-1640 medium overnight. A culture medium of RPMI-1640 with addition of 10% fetal bovine serum (FBS), amphotericin B (2.5 µg/mL), penicillin (100 units/mL),

streptomycin (100 µg/mL) and phorbol 12 myristate 13 acetate (PMA) (10 ng/mL) was prepared. THP-1 cells, a human monocytic cell line, were differentiated into adherent macrophage-like cells using PMA. To differentiate THP-1 cells into M1 and M2 phenotypes, the bulk medium was supplemented with lipopolysaccharide (LPS) (100 ng/mL) and interferon gamma (IFN-γ) (50 ng/mL) to differentiate a M1 phenotype, or interleukin 4 (IL-4) (10 ng/mL) to differentiate a M2 (specifically M2a) phenotype^{32,34} THP-1 cells were grown to passage 15 and viability was determined using Trypan Blue exclusion (Sigma Aldrich, UK), which was typically >95%. A starting concentration of 6.7×10^5 cells/mL was used. 1.5 mL of the cell suspension was incubated in wells with each metal disc. Cell culture medium was also incubated with the metal samples as a control condition. Control groups with no metal discs were also prepared in parallel, containing 1.5 mL of M1 cells with the bulk medium, 1.5 mL of M2 cells with the bulk medium and the bulk medium alone respectively. Six groups of incubation assays, with triplicated samples for each group, were incubated in a thermostatic incubator at 37 °C, 5% CO₂ and 100% humidity. After 4 days of incubation, 1 mL of medium was removed from each well and replaced with 1 mL of fresh medium with appropriate cytokines. The extracted media from the wells were individually stored and frozen at -20 °C. This process was repeated 3 times for each consecutive 4-day period. At the end of 13 days incubation, 60 µL of detergent (10% sodium dodecyl (lauryl) sulfate (SDS)) was added into all wells (including the control groups) and 1.5 mL medium which included supernatants and cell lysates were collected from each well and frozen at -20 °C.

For inductively coupled plasma-mass spectroscopy (ICP-MS) analysis, the 3 media aliquots (3 mL) collected during the incubation and the 1.5 mL aliquot collected at the end of incubation were pooled together, from which 3.4 mL was taken for solution analysis.

2.5 Quantification of metal ion release

The retrieved and pooled sample solutions were refrigerated at -20 °C prior to analysis. The metal ion concentrations of Ti and Zr were quantified from neat sample solutions using a Thermo iCAPTM 7000 ICP-AES system (Thermo Fisher Scientific, UK), which was calibrated against serially diluted Ti and Zr standards (Fisher Scientific, UK). The system was rinsed with 10% HNO₃ in between analyzed samples. The detection limit was 0.3 ppb for Ti and 0.4 ppb for Zr.

2.6 Surface Characterisation

Cell adherence and the cell morphologies of THP-1 cells on each metal substrate were characterised using scanning electron microscopy (SEM) (Zeiss EVO MA-10) in secondary electron mode with an energy of 10 keV. Surface coverage of cells (which was considered to reflect the percentage of surface exposed to cell-generated ROS species) was examined by SEM imaging of the retrieved metal substrates after culturing with unstimulated THP-1 cells, for 7 days for each alloy composition. Morphologies of M1 and M2 phenotypes of THP-1 cells were characterised on retrieved CP Ti substrates after culturing with the cells in respective stimulating media for 24 h. All the retrieved discs were prepared by fixation and dehydration method prior to SEM characterisation. The retrieved metal substrates with adhered cells were washed with Hank's balanced salt solution (Sigma Aldrich, UK) gently for 3 times and fixed by incubation in 1.5 mL of 2.5% glutaraldehyde (EM Grade, Agar Scientific, UK) in 0.1 M sodium cacodylate for 10 mins at room temperature. The disks were then dehydrated by sequential immersion in 1 mL of 20%, 30%, 40%, 50%, 60%, 70%, 90%, 95%, 100% (twice) ethanol for 10 min, followed by incubating with 0.2 mL of hexamethyldisilazane which was allowed to evaporate overnight.

Image analysis on standardised SEM images (cell morphology and surface coverage) was performed using Fiji software (ImageJ, National Institutes of Health, USA) using the method described previously.³⁵ The cells were segmented from the surface using the Trainable Weka Segmentation plugin³⁶ with segmentation filters as previously described.^{35, 37} After segmenting each image (four in images for each cell phenotype), objects that were less than 30 pixels were assumed to be noise and were removed using ‘Analyse Particles’ plugin.³⁵ The image histogram was calculated to determine the number of pixels corresponding to cell coverage. This value was used along with the total number of pixels in the image to calculate the amount of cells covering the surface as a percentage of the total area in the image, termed the ‘cell spread area’. Statistical difference was tested by one-way analysis of variance (ANOVA) at a significance level of $\alpha=0.05$.

3 RESULTS

3.1 Microstructure

Optical micrographs of etched CP Ti and binary TiZr alloys discs are shown in **Figure 1**. CP Ti consists of equiaxed α grains. Ti5Zr has coarse as-cast grains within which there are primary α lamellae in colonies. With increases in Zr, as seen in the case for Ti15Zr and Ti50Zr, finer needle-type lamellae structures are exhibited. The structure of Zr is shown in an SEM image (Figure 1) on an as-polished surface instead of an etched surface as Zr was unsuitable for etching in Kroll's solution. The CP Zr surface showed features of α grains with a uniform distribution of second phase particles, with a size of 1-5 μm , that were confirmed to be enriched in Fe and depleted in Zr by EDX analysis.

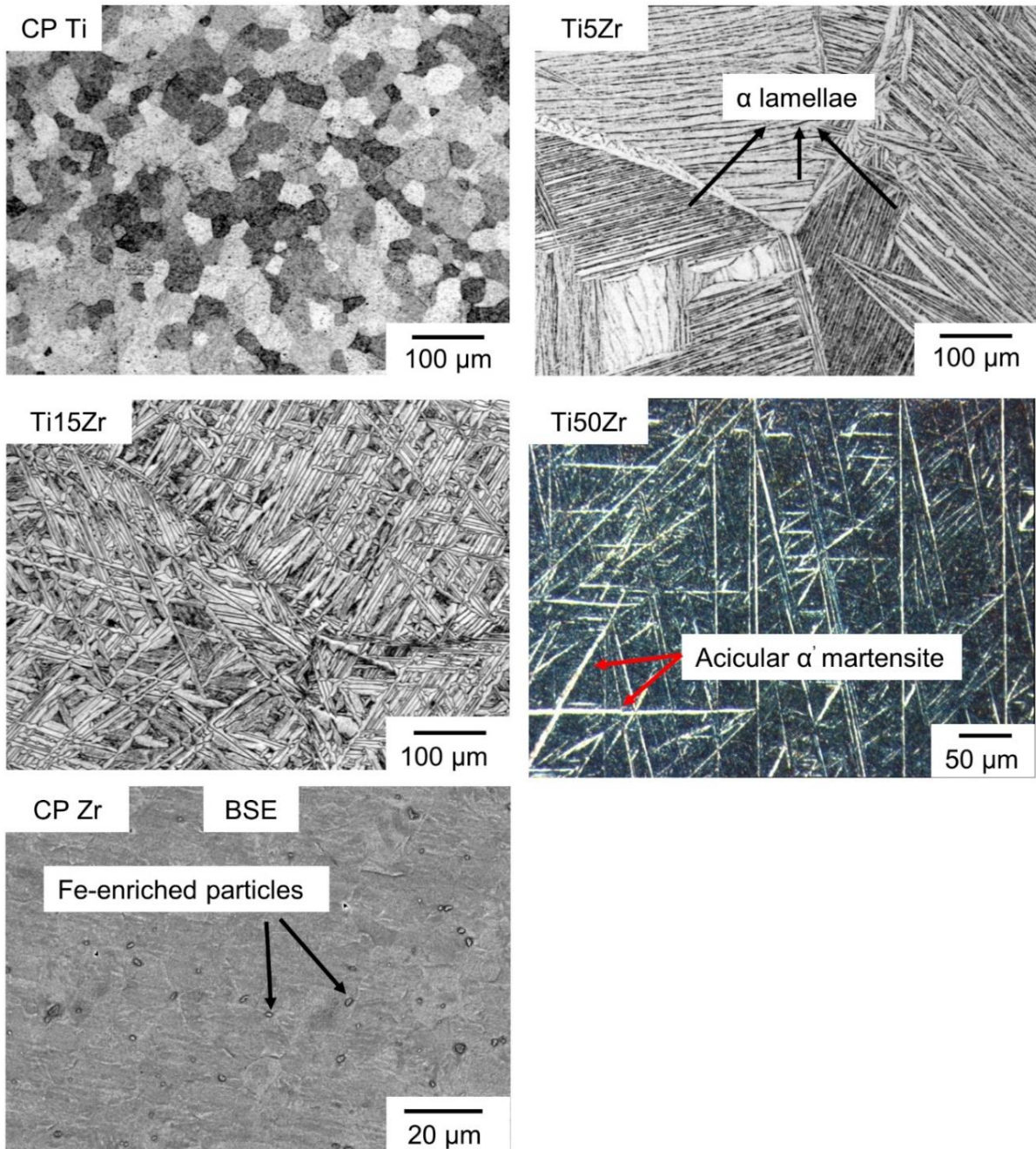


Figure 1. Optical microscopy images of the etched surfaces of CP Ti, Ti5Zr, Ti15Zr and Ti50Zr (all in at%). SEM (BSE) image of an as-polished surface of CP Zr featuring characteristics of second phase particles, which were shown to be enriched in Fe and depleted in Zr by EDX examination.

3.2 Corrosion behaviour in HCl

Open circuit potentials (OCPs) of CP Ti, TiZr binary alloys and CP Zr in 2 M HCl solutions are shown in **Figure 2a**. The OCP for CP Ti showed rapid decrease with time from ~ -350 mV, then settled close to -650 mV, consistent with a depassivation. Ti5Zr also showed an abrupt decrease in OCP, but the timescale was significantly longer than that for CP Ti and the OCP after 1 hour was slightly higher at ~ -600 mV. Ti15Zr showed a much more gradual decrease in OCP to ~ -400 mV whereas Ti50Zr and CP Zr both showed a gradual increase in OCP to ~ -300 mV and ~ -230 mV, respectively indicating surface passivation.

Anodic polarisation curves of the alloys after 1 h immersion in 2 M HCl solutions at OCP are shown in **Figure 2b**. CP Ti exhibited a clear active/passive transition at -500 mV with an anodic peak of critical current density (i_{crit}) of $\sim 60 \mu\text{A}/\text{cm}^2$, whereas Ti5Zr showed a similar active passive transition but with a reduced i_{crit} of $\sim 40 \mu\text{A}/\text{cm}^2$. There is no sign of any increased current density at high potential associated with pitting corrosion. Ti15Zr did not show an active-passive transition but instead showed only a passive region with a passive current density of $\sim 10 \mu\text{A}/\text{cm}^2$ without any sign of pitting corrosion at potentials up to 1.4 V. Ti50Zr showed similar passive behaviour with a lower passive current density of $\sim 5 \mu\text{A}/\text{cm}^2$ compared with Ti15Zr, however it was susceptible to pitting corrosion, shown by a sudden increase in current at higher potential. The pitting potential was variable with one value 640 mV and the other above 1000 mV. Similarly, CP Zr was even more susceptible to pitting at much lower potentials at approximately 100 mV. It can be concluded that at potentials before pitting breakdown, with increasing additions of Zr in Ti, the passive current densities were progressively reduced, showing enhancement of the passivity and thus corrosion resistance of Ti.

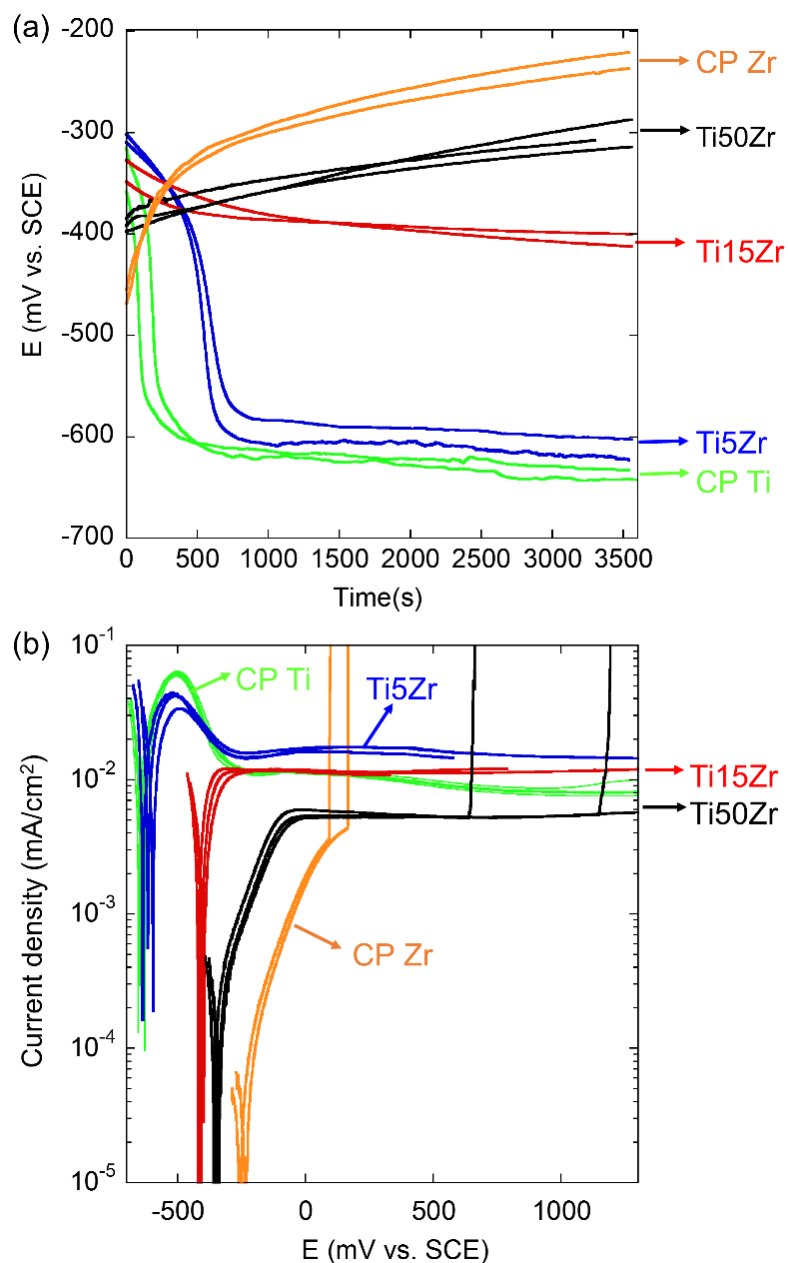


Figure 2. (a) Open Circuit Potentials of CP Ti, Ti5Zr, Ti15Zr, Ti50Zr alloys and CP Zr in 2 M HCl during 1 h immersion at 37 °C; (b) Anodic polarisation of CP Ti, Ti5Zr, Ti15Zr, Ti50Zr alloys and CP Zr in 2 M HCl at 37°C after 1 h immersion at OCP. Scan rate was 1 mV/s.

3.3 Corrosion behaviour in physiological saline with and without H₂O₂

The OCP as a function of time was measured for CP Ti, TiZr alloys and CP Zr in 0.9% NaCl with and without the addition of 0.1 M H₂O₂. For all of the measurements, the OCP gradually

increased during the 1 h immersion period (not shown), indicating passivation. **Figure 3** shows the OCP at 1 h as a function of Zr concentration. It can be seen that in both solutions, the OCP is significantly higher in the presence of H₂O₂. Both in the presence and absence of H₂O₂, addition of 5% Zr decreases the OCP significantly, with a further decrease for Ti15Zr, and smaller decreases for higher Zr levels.

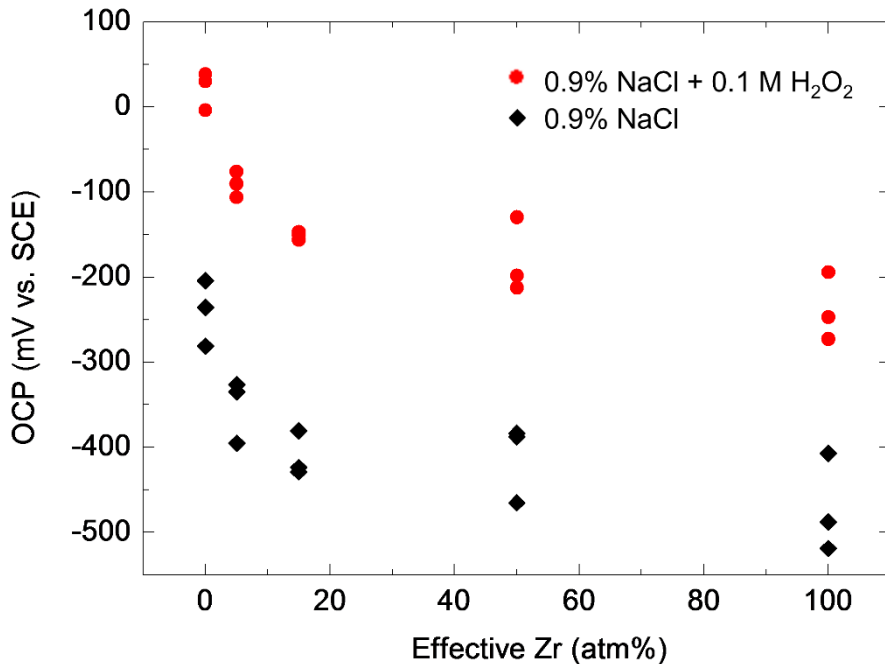


Figure 3. OCP of CP Ti, Ti5Zr, Ti15Zr, Ti50Zr and CP Zr in physiological saline (0.9% NaCl) with or without addition of 0.1 M H₂O₂ after 1h immersion at 37 °C. The x-axis is the effective Zr concentration (at%) in each tested alloy. All data shown (n=3).

Anodic polarisation curves for CP Ti, TiZr alloys and CP Zr were measured in 0.9% NaCl solutions with and without addition of H₂O₂ (**Figure 4**). In 0.9% NaCl solution alone, it was found that CP Ti, Ti5Zr and Ti15Zr showed spontaneous passivation with passive current densities at a similar level (5 $\mu\text{A}/\text{cm}^2$) and no anodic breakdown was observed for potentials up to 1000 mV. Ti50Zr and CP Zr also showed spontaneous passivation with a similar passive current density but both were susceptible to pitting at potentials > 500 mV.

In 0.9% NaCl with addition of 0.1 M H₂O₂, spontaneous passivation was again observed in CP Ti, Ti5Zr and Ti15Zr and the passive current densities were increased by up to 3 μA/cm² in relative to the level of 5 μA/cm² observed without the addition of H₂O₂. However, for Ti50Zr and CP Zr, such increases were not observed and passive current densities were reduced compared to the level of 5 μA/cm² in the absence of H₂O₂. Pitting behaviour was observed at high potentials (close to 1000 mV) in both Ti50Zr and CP Zr, indicating a similar susceptibility to pitting in 0.9% NaCl regardless of the presence and absence of H₂O₂.

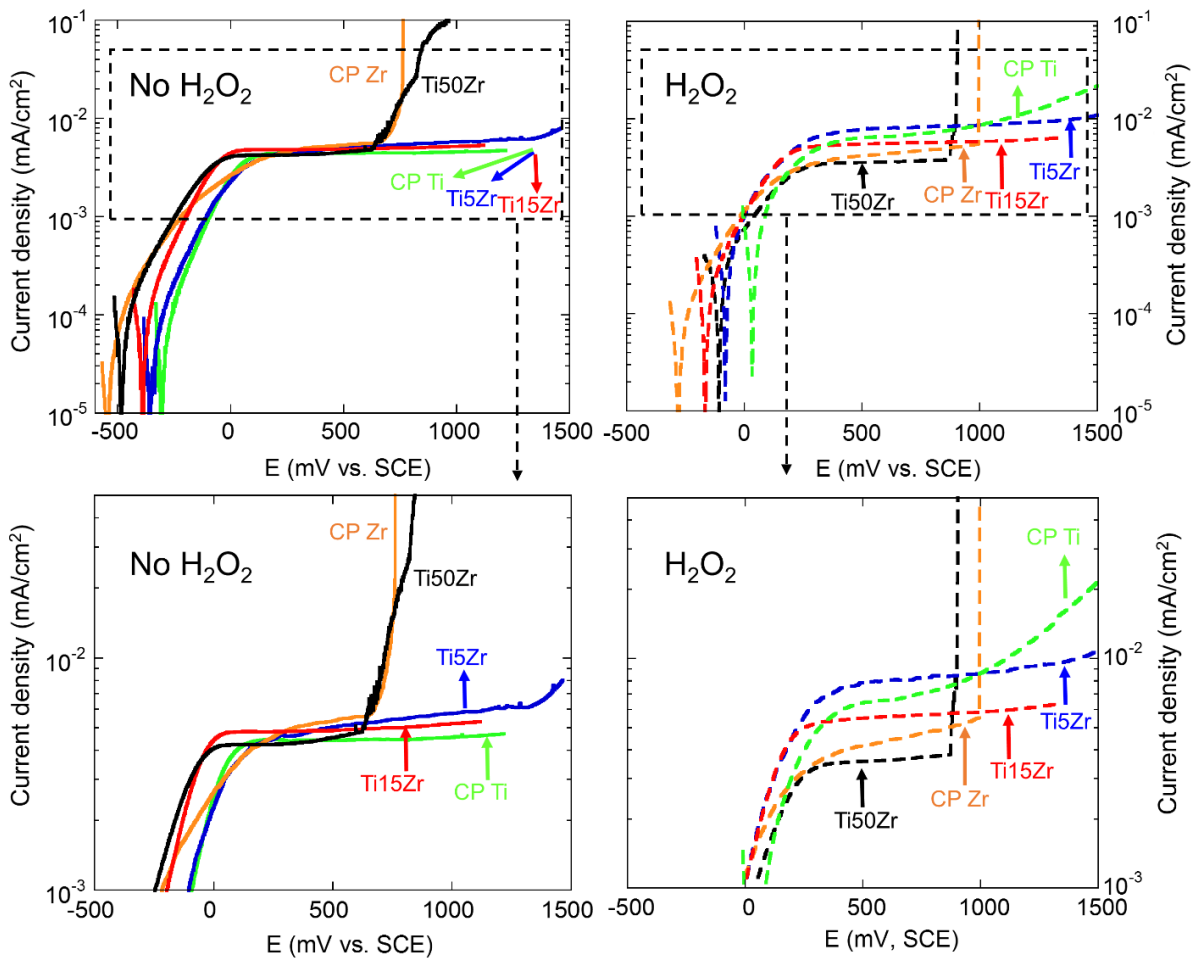


Figure 4. Anodic polarisation of CP Ti, Ti5Zr, Ti15Zr, Ti50Zr alloys and CP Zr in 0.9% NaCl with and without addition of 0.1 M H₂O₂ at 37 °C after 1 h immersion at OCP. Scan rate was 1 mV/s.

Cathodic polarisation curves of CP Ti, TiZr alloys and CP Zr were measured in 0.9% NaCl with and without addition of H₂O₂ and are shown in **Figure 5**. It was observed that in 0.9% NaCl alone, the addition of Zr to Ti reduced the cathodic current density. In 0.9% NaCl with the addition of 0.1 M H₂O₂, the rates for cathodic reactions were increased for all alloys due to reduction of H₂O₂. Addition of Zr to Ti decreased the cathodic reaction rates in solutions of 0.9% NaCl containing H₂O₂.

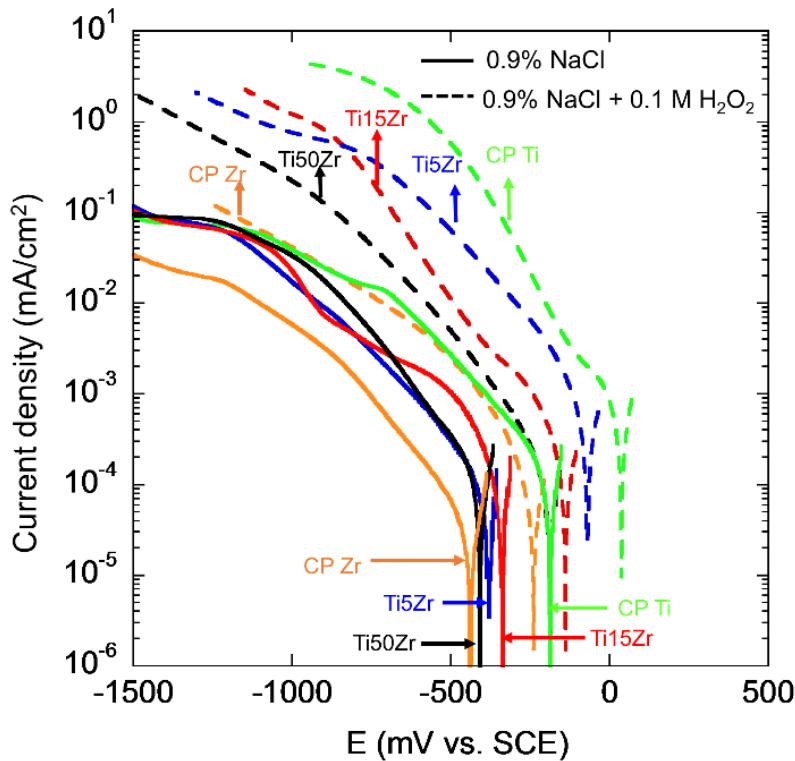


Figure 5. Cathodic polarisation curves for CP Ti, Ti5Zr, Ti15Zr, Ti50Zr and CP Zr in 0.9% NaCl with and without addition of 0.1 M H₂O₂ at 37 °C after 1 h immersion at OCP. Scan rate was 1 mV/s.

Potentiostatic polarisation experiments (**Figure 6**) were carried out in 0.9% NaCl at 500 mV, which is a potential in the passive region (Figure 4). At ~1000 s, in some cases H₂O₂ was added to give a final concentration of 0.1 M H₂O₂ in 0.9% NaCl, and all solutions were stirred at this point. CP Zr underwent pitting after polarisation and is therefore not included in Figure 6. For all alloys in solutions that were only stirred, without addition of H₂O₂ (solid lines in Figure 6),

the current density continued to decrease, consistent with a growing passive film. When H_2O_2 was added, the current densities for CP Ti and Ti5Zr started to increase (broken lines in Figure 6), suggesting that the passive films became less protective. The increase in current density following addition of H_2O_2 was less for Ti15Zr, and for Ti50Zr, the effect of H_2O_2 was completely suppressed.

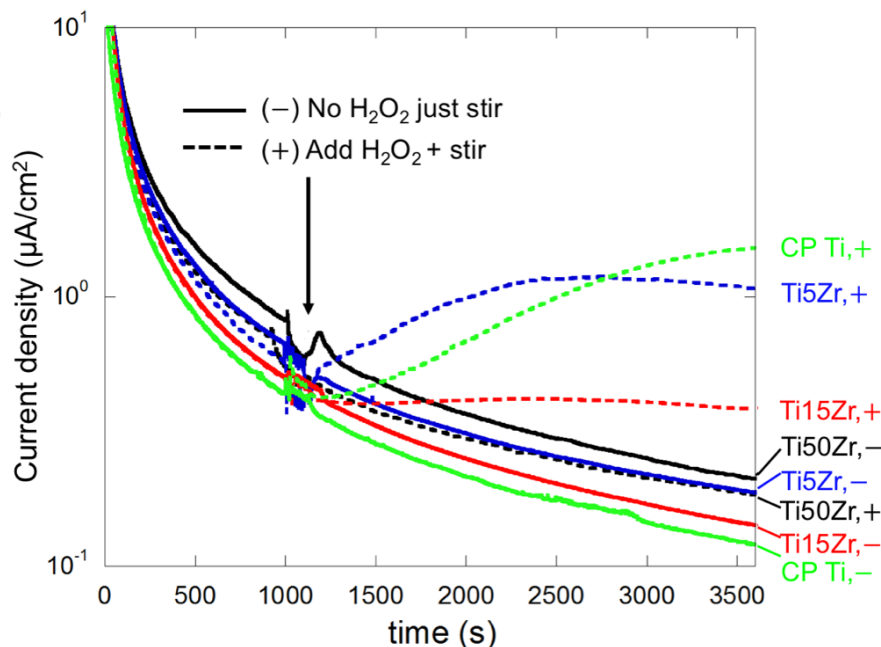


Figure 6. Current density as a function of time for CP Ti, Ti5Zr, Ti15Zr, Ti50Zr and CP Zr under potentiostatic control at 500 mV (vs. SCE) in 0.9% NaCl after 1 h immersion at OCP, 37 °C. For some experiments, H_2O_2 was added to the solution to give a final concentration of 0.1 M H_2O_2 at 1000 s (broken lines), and in all experiments, the solution was stirred just after 1000 s.

3.4 Metal ion release associated with THP 1 culture

Quantitative image analysis of adherent THP-1 cells on Ti, Zr, TiZr surfaces confirmed minor differences in surface coverage between different substrates, varying from 74% (Ti50Zr alloy) to 92% (Ti15Zr alloy) between the five types of alloys. On the CP Ti surface, THP-1 cells differentiated into M1 and M2 phenotypes showed morphological differences (**Figure 7**). M1 cells exhibited round flattened shapes (Figure 7a) and M2 cells showed elongation (Figure 7d).

Cell coverage on the CP Ti surface differed between M1 and M2 phenotypes with the M1 cells demonstrating a significantly lower cell spread area ($50\% \pm 13\%$) compared to the M2 phenotype ($82\% \pm 2\%$) ($p=0.02$).

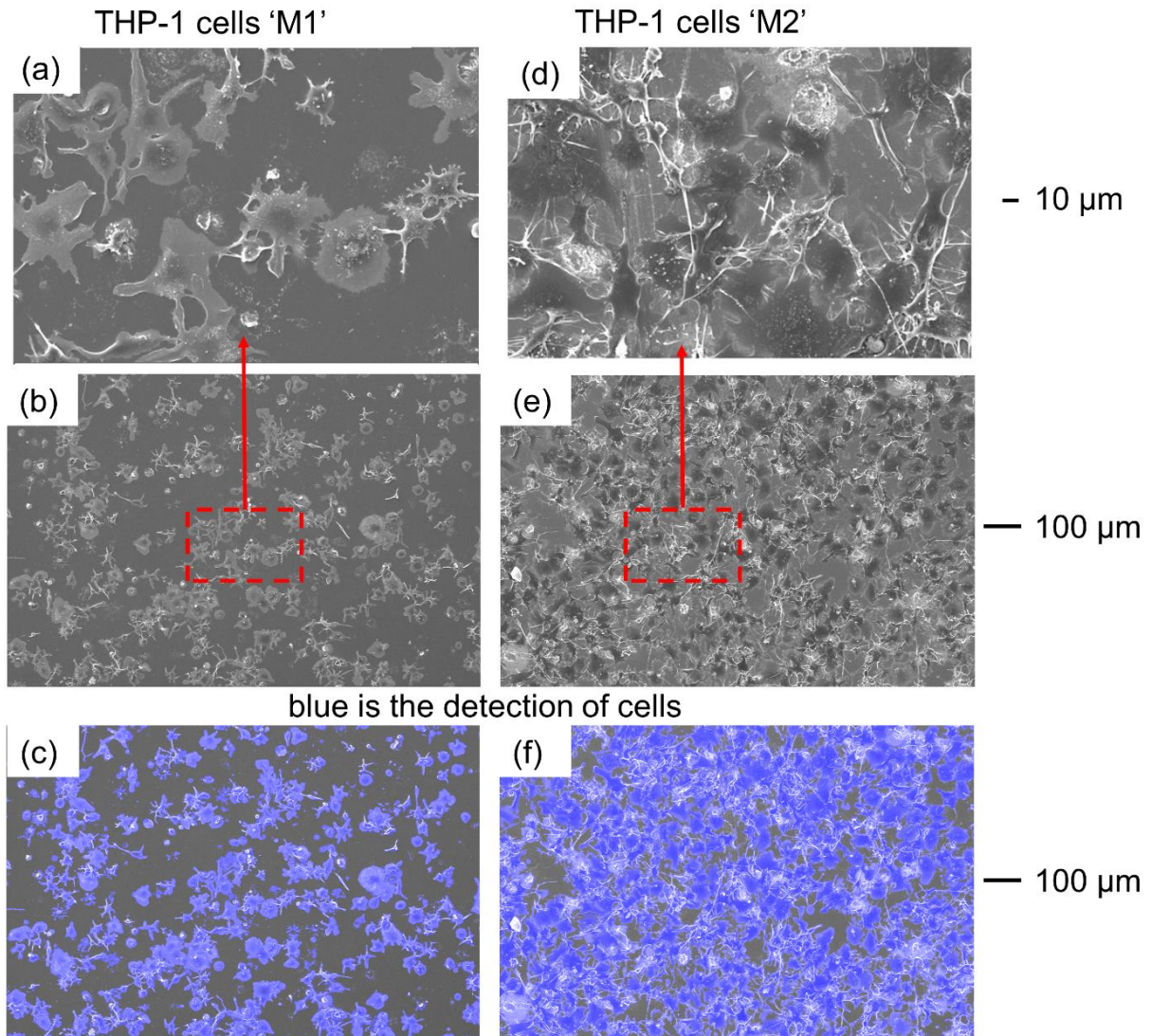


Figure 7. SEM images of (a)-(c), M1 phenotype of THP-1 cells stimulated with PMA, IFN- γ and LPS; (d)-(f) M2 phenotype of THP-1 cells, stimulated with PMA and IL-4 on the CP Ti G2 metal substrate. The first row is the magnified area of SEM images, in the second row; the third row in blue is the detection of cells (by image segmentation, Fiji analysis software) on the metal substrates.

Figure 8 shows the metal ions released from alloys incubated in THP-1 macrophage cell culture of M1 (pro-inflammatory pathways) or M2 (tissue repair) phenotypes for 13 days. The

metal ions released are normalised to the fraction of the metal in the alloy. Figure 8a shows that significant levels of Ti ions are released from all of the alloys in the presence of the ROS-generating macrophages compared with the control experiments where the metals are exposed only to growth medium in the absence of macrophages. Furthermore, the amount of released titanium decreases significantly as the fraction of Zr in the alloy is increased. This is particularly clear when the data from both macrophage cultures are added together.

Normalised Zr ion release from TiZr alloys (5%, 15% and 50% Zr) and CP Zr is shown in Figure 8b. Zr release was shown to be lower than Ti release as data are normalised to the at% composition of each exposed alloy.

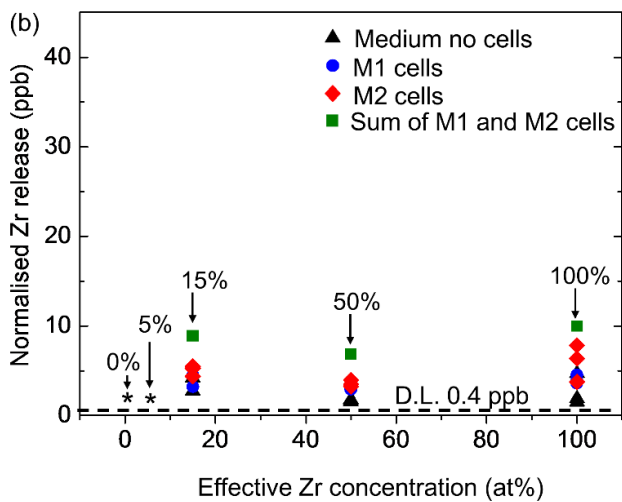
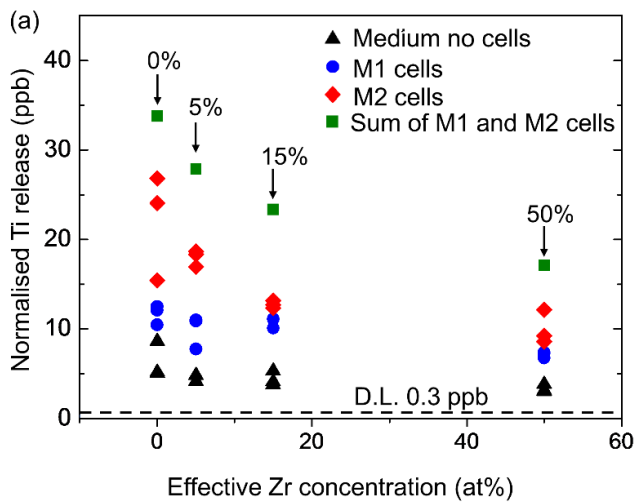


Figure 8. Normalised (by concentration, at%, in respective alloys) (a) Ti release (ppb) (b) Zr release (ppb) from immersed alloys CP Ti, Ti5Zr, Ti15Zr, Ti50Zr and CP Zr after 13 days of incubation in RPMI 1640 medium with or without addition of M1 or M2 phenotype THP-1 cells at 37 °C, 5% CO₂, 100% humidity. All data shown (n=3). Square markers for ‘sum of M1 and M2 THP1 cells’ are total of two average values of metal releases under M1 or M2 conditions. Detection limit (D.L.) was 0.3 ppb for Ti and 0.4 ppb for Zr. Marker (*) indicates measurements made for CP Ti (0%) and Ti5Zr (5%) were below the detection limit.

4 DISCUSSION

4.1 Zr additions reduced passive current density of Ti in HCl solutions

Previously it has been established that Ti oxides became destabilised when exposed to concentrated reducing acids like HCl,^{10, 38} and the addition of 50% Zr to Ti improved its oxide stability at open circuit¹⁰ and increased its resistance to dissolution at lower potentials.¹¹ The present study is consistent and supports previous findings. In addition, it was observed that at open circuit conditions (Figure 2a) the addition of 5% Zr to Ti showed little differences compared with CP Ti. However, with 15% addition of Zr to Ti, a much bigger difference was presented where the characteristic abrupt drops associated with oxide film dissolution¹⁰ were not shown, implying an enhanced surface oxide stability. Further increased Zr additions to Ti (50% and 100%, effectively), in contrast, demonstrated spontaneous passivation behaviour, where it was suggested that Zr oxides are kinetically resistant to chemical dissolution in HCl solutions.¹⁰

CP Ti is susceptible to dissolution at low potentials (Figure 2b), which can be established by dissolution or rupture of passive films which is encountered in mechanically-assisted crevice corrosion.¹⁹ In contrast, Zr (and ZrO₂) was shown to be resistant to dissolution in the acidic environment at low potentials.¹¹ Addition of 5 at% Zr suppressed the active dissolution peaks and was observed with a reduced critical current density, indicating an increased resistance to dissolution. For 15 at% Zr and above, the surface oxide films preserved following immersion at

OCP in 2 M HCl, resulting in spontaneous passivation during polarisation (Figure 2b). It can be concluded that increasing Zr additions to Ti enhances its passivity at low potentials in acidic environments. This can be attributed to the different resistance of TiO_2 and ZrO_2 to dissolution at low potentials, where TiO_2 can be preferentially dissolved resulting in accumulation of ZrO_2 in the surface oxides,¹¹ making it more resistant to dissolution.

4.2 Zr contents increased corrosion resistance of CP Ti in physiological saline with H_2O_2

In the neutral environment (physiological saline with or without addition of 0.1 M H_2O_2), spontaneous passivation was observed for all alloys at open circuit conditions. The addition of H_2O_2 increased the OCP of all the alloys (Figure 3), since H_2O_2 is a strong oxidant³⁹ and enhanced the cathodic activities of all the alloys (Figure 5). Increasing Zr additions in Ti progressively reduced the potentials in both H_2O_2 free and H_2O_2 containing electrolytes. This was due to the reduced rates of cathodic reactions of TiZr alloys with increasing Zr additions, which is likely to be a result of the formation of a thicker and less conductive oxide (Figure 5).

It is well-established that H_2O_2 enhances the corrosion of Ti via a complexation reaction with its surface oxides.^{17, 22-26} Consistently in the present work, higher passive densities of Ti were observed following the introduction of H_2O_2 in the saline during both potentiodynamic and potentiostatic polarisations (Figure 4 and Figure 6). However, increasing additions of Zr (from 5% to 50%) in Ti presented reduced scales of increased passive current densities (Figure 4). Furthermore, it was observed a progressive suppression in the impact of H_2O_2 on the rise in passive current density at a static potential (Figure 6), by increasing additions of Zr in Ti. A complete passivation behaviour was found with the 50% Zr addition regardless the presence of H_2O_2 . It appears that Zr and/or Zr oxides are not susceptible to the complexation by H_2O_2 , which

seems to protect the surface oxide of TiZr alloy by forming a ZrO₂-enriched surface film that is resistant to dissolution in the presence of H₂O₂.

4.3 Increased pitting susceptibility by higher Zr concentrations in Ti

Increased pitting susceptibilities were observed with higher Zr additions in Ti including Ti50Zr as well as CP Zr in both acidic (HCl) and neutral (physiological saline with and without H₂O₂) solutions (Figure 2b and Figure 4). It was found that Ti50Zr was susceptible to pitting at potentials >500 mV in both HCl and physiological saline. However, CP Zr showed much lower pitting potentials in the HCl (around 100 mV) than those in the NaCl (>500 mV), indicating higher pitting susceptibility at lower pH. It is well known that Ti has a high level of resistance to pitting corrosion and a recent study on the corrosion of Ti and Ti-Zr alloys in a lactic acid solution and artificial saliva found that Ti-30Zr and Ti-50Zr were resistant to pitting corrosion whereas Ti-70Zr was susceptible.⁴⁰ Zr is known to be vulnerable to pitting attack in chloride containing environments,^{41, 42} and pits are often found initiated at the flaws of the metal, such as the Fe-enriched second phase particles observed on the CP Zr surface (Figure 1), which could account for the observed pitting susceptibility.

4.4 Zr additions enhance cell mediated corrosion resistance

Corrosion mediated by the contents of microenvironments formed between eukaryotic or prokaryotic cells and implant surfaces has been associated with implant degradation *in vivo*.^{21, 27, 28} Cell mediated corrosion has been linked to cellular production of ROS species, including superoxide anions and H₂O₂ released or formed in the environmental niche between a metal surface and the adhered cells.^{21, 27} The presence of adherent THP-1 cells resulted in both Ti and Zr release (Figure 8). Different functional phenotypes of THP-1 cells resulted in differences in metal releases. M1 or M2 macrophage phenotypes can be distinguished by their different ability

to produce inflammatory cytokines as well as oxygen and nitrogen radicals.⁴³ The pro-inflammatory M1 state is a classically activated state with enhanced microbicidal activities including ROS production (to increase killing ability).^{43, 44} The M2 state is associated with a wound-healing phenotype of macrophages, which is less efficient in producing ROS species than the M1 state.⁴³ It is worth pointing out the activity of the cells and ROS release are directly associated with functional activity such as phagocytosis, which was not simulated in this study. Here, Ti release was found to be higher in the presence of THP-1 cells in their M2 state when compared with the activated M1 state (Figure 8), which might be considered counter-intuitive given the higher ROS levels often associated with M1 macrophages. However, it should be noted that M2 macrophages are also capable of ROS production, albeit less than M1 macrophages.³³ M2 macrophages are also phenotypically related to Foreign Body Giant Cells (FBGC),⁴⁵ and both M2 and FBGC can be derived from monocytes by IL-4 treatment.⁴⁶ FBGC are multinucleate syncytial cells formed by fusion of multiple macrophages in response to foreign bodies such as biomaterials which are too large to be phagocytosed,⁴⁷ and share characteristics of both M1 and M2 macrophages.^{45,48} FBGC generate a sealed cavity between themselves and the surface of foreign material, into which they secrete enzymes and ROS. This process, termed frustrated phagocytosis, has been observed in THP-1 cells exposed to non-phagocytosable synthetic materials.⁴⁹

In addition, the extracellular chemistry is complex in nature⁴³ and the concentration of ROS species such as H₂O₂ can vary with time and spatially.⁵⁰ The enhanced metal ion release by M2 cells in this study is most likely attributed to the significantly higher surface coverage observed by the cells on the metal surface creating the micro-environments that permit interactions between ROS and the substrate surface (Figure 7). It was found that Ti dissolution induced by

M2 cells was suppressed progressively by the addition of Zr (Figure 8), similarly shown in the sum of averaged metal release induced by M1 and M2 cells, which was found to be entirely consistent with the inhibiting effect of Zr addition on dissolution of Ti in the presence of H₂O₂ (Figure 6) and in HCl solutions (Figure 2). The effect of Zr additions in Ti has been demonstrated to enhance the corrosion resistance and passivity of Ti in both acidic (HCl) and inflammatory (H₂O₂ in 0.9% NaCl) environments. Consistently in more physiologically representative cell cultures, increasing Zr additions in Ti has been demonstrated to significantly reduce Ti ion release. However, the optimized Zr content in the TiZr alloy should be based on the balance of enhanced passivity at low potentials and enhanced pitting resistance at high potentials.⁴⁰ It is suggested that the optimal range of Zr proportion will be less than 50%,⁴⁰ and in this study the Ti15Zr alloy exhibited optimum behavior.

5 CONCLUSIONS

1. Additions of Zr to Ti (systemically from 5, 15, 50%) have been shown to induce significant effects on corrosion resistance of Ti:
 - a) in acidic environment (2 M HCl), additions of Zr enhance oxide film stability and passivity of Ti.
 - b) in H₂O₂ containing 0.9% NaCl solutions (representative of a more inflammatory environment), additions of Zr reduce OCPs of Ti by decreasing its cathodic activities. Furthermore, the enhanced anodic dissolution of Ti induced by H₂O₂ were suppressed progressively by increasing Zr additions, suggesting a more resistant surface oxide film of TiZr alloy compared with CP Ti.
 - c) However, higher addition of Zr e.g. 50 at% in Ti was susceptible to pitting at high potentials in both HCl and H₂O₂ containing NaCl solutions.

2. Ti release from CP Ti and TiZr alloys was induced by the presence of adherent THP-1 cells inducted into a pro-inflammatory M1 phenotype and into a 'tissue healing' M2 phenotype. The magnitude of ion release was reduced with increasing Zr content and the pattern of corrosion behaviour was consistent with electrochemical measurements.
3. Systematic addition of Zr to Ti has been demonstrated to progressively enhance Ti passivity in both simulated physiological solutions and cell-culture environment. However, caution needs to be taken when considering higher Zr concentrations due to an increased susceptibility to pitting corrosion. Optimisation of composition should be based on both passivity and pitting resistance such as Ti15Zr found in this study.

AUTHOR INFORMATION

Author Contributions

Y.Z., O.A. and A.D. conceived the project and designed the experiments. Y.Z. performed the experiments, analyzed and interpreted the data. B.B. contributed to design and perform the cell culture immersion experiments. N.V. contributed to the methodology of cell image analysis. Y.Z. wrote the manuscript and O.A. with other authors contributed to the critical reading and revision of the manuscript. All authors have given approval to the final version of the manuscript.

Funding Sources

O. Addison was funded by the National Institute for Health Research, award No. NIHR/CS/010/001. This article presents independent research funded by the National Institute for Health Research (NIHR). The views expressed are those of the author(s) and not necessarily those of the NIHR.

Notes

The authors declare no competing financial interest.

ACKNOWLEDGMENT

Y. Zhang received postgraduate research scholarship by School of Metallurgy and Materials in University of Birmingham and O. Addison was funded by the National Institute for Health Research, award No. NIHR/CS/010/001.

ABBREVIATIONS

ROS, Reactive Oxygen Species; RPMI-1640, Roswell Park Memorial Institute-1640 (cell culture medium); FBS, Fetal Bovine Serum; PMA, phorbol 12 myristate 13 acetate; LPS,

lipopolysaccharide; IFN- γ , interferon gamma; IL-4, interleukin 4; SDS, sodium dodecyl (lauryl) sulfate; EDX, Energy Dispersive X-ray analysis; SEM, Scanning Electron Microscopy; OCP, Open Circuit Potentials; SCE, Standard Calomel Electrode; ICP-AES, Inductively Coupled Plasma-Atomic Emission Spectroscopy; MACC, Mechanically-Assisted Crevice Corrosion.

REFERENCES

1. Lemons, J. E.; Misch-Dietsh, F.; McCracken, M. S. In *Dental Implant Prosthetics*, 2nd ed.; Misch, C. E., Ed.; Mosby: St. Louis, 2015; p 66. DOI: 10.1016/B978-0-323-07845-0.00004-X
2. Grandin, H. M.; Berner, S.; Dard, M. A Review of Titanium Zirconium (TiZr) Alloys for Use in Endosseous Dental Implants. *Materials* **2012**, *5*, 1348-1360. DOI: 10.3390/ma5081348
3. Ho, W.-F.; Chen, W.-K.; Wu, S.-C.; Hsu, H.-C. Structure, Mechanical Properties, and Grindability of Dental Ti–Zr Alloys. *J. Mater. Sci.: Mater. Med.* **2008**, *19*, 3179-3186. DOI: 10.1007/s10856-008-3454-x
4. Kobayashi, E.; Matsumoto, S.; Doi, H.; Yoneyama, T.; Hamanaka, H. Mechanical Properties of the Binary Titanium-Zirconium Alloys and their Potential for Biomedical Materials. *J. Biomed. Mater. Res.* **1995**, *29*, 943-950. DOI: 10.1002/jbm.820290805
5. Takahashi, M.; Kikuchi, M.; Okuno, O. Grindability of Dental Cast Ti-Zr Binary Alloys. *J. Jpn. Inst. Met.* **2010**, *74*, 351-355. DOI: 10.2320/jinstmet.74.351
6. Parr, G. R.; Gardner, L. K.; Toth, R. W. Titanium: the Mystery Metal of Implant Dentistry. Dental Materials Aspects. *J. Prosthet. Dent.* **1985**, *54*, 410-414. DOI: 10.1016/0022-3913(85)90562-1

7. Pound, B. G. Passive Films on Metallic Biomaterials Under Simulated Physiological Conditions. *J. Biomed. Mater. Res., Part A* **2014**, *102*, 1595-1604. DOI: 10.1002/jbm.a.34798
8. Mamun, A.; Schennach, R.; Parga, J. R.; Mollah, M. Y. A.; Hossain, M. A.; Cocke, D. L. Passive Film Breakdown During Anodic Oxidation of Zirconium in pH 8 Buffer Containing Chloride and Sulfate. *Electrochim. Acta.* **2001**, *46*, 3343-3350. DOI: 10.1016/S0013-4686(01)00544-8
9. Moreno, J. M. C.; Vasilescu, E.; Drob, P.; Osiceanu, P.; Vasilescu, C.; Drob, S. I.; Popa, M. Surface Analysis and Electrochemical Behavior of Ti-20Zr Alloy in Simulated Physiological Fluids. *Mater. Sci. Eng., B* **2013**, *178*, 1195-1204. DOI: 10.1016/j.mseb.2013.07.006
10. Yu, S. Y.; Brodrick, C. W.; Ryan, M. P.; Scully, J. R. Effects of Nb and Zr Alloying Additions on the Activation Behavior of Ti in Hydrochloric Acid. *J. Electrochem. Soc.* **1999**, *146*, 4429-4438. DOI: 10.1149/1.1392655
11. Yu, S. Y.; Scully, J. R.; Vitus, C. M. Influence of Niobium and Zirconium Alloying Additions on the Anodic Dissolution Behavior of Activated Titanium in HCl Solutions. *J. Electrochem. Soc.* **2001**, *148*, B68-B78. DOI: 10.1149/1.1337605
12. Zhang, Y. M.; Chai, F.; Hornez, J. C.; Li, C. L.; Zhao, Y. M.; Traisnel, M.; Hildebrand, H. F. The Corrosion and Biological Behaviour of Titanium Alloys in the Presence of Human Lymphoid Cells and MC3T3-E1 Osteoblasts. *Biomed. Mater.* **2009**, *4*. DOI: 10.1088/1748-6041/4/1/015004

13. Han, M.-K.; Hwang, M.-J.; Yang, M.-S.; Yang, H.-S.; Song, H.-J.; Park, Y.-J. Effect of Zirconium Content on the Microstructure, Physical Properties and Corrosion Behavior of Ti Alloys. *Mater. Sci. Eng., A* **2014**, *616*, 268-274. DOI: 10.1016/j.msea.2014.08.010
14. Mareci, D.; Bolat, G.; Cailean, A.; Santana, J. J.; Izquierdo, J.; Souto, R. M. Effect of Acidic Fluoride Solution on the Corrosion Resistance of ZrTi Alloys for Dental Implant Application. *Corros. Sci.* **2014**, *87*, 334-343. DOI: 10.1016/j.corsci.2014.06.042
15. Mareci, D.; Bolat, G.; Chelariu, R.; Sutiman, D.; Munteanu, C. The Estimation of Corrosion Behaviour of ZrTi Binary Alloys for Dental Applications Using Electrochemical Techniques. *Mater. Chem. Phys.* **2013**, *141*, 362-369. DOI: 10.1016/j.matchemphys.2013.05.024
16. Izquierdo, J.; Bolat, G.; Mareci, D.; Munteanu, C.; González, S.; Souto, R. M. Electrochemical Behaviour of ZrTi Alloys in Artificial Physiological Solution Simulating In Vitro Inflammatory Conditions. *Appl. Surf. Sci.* **2014**, *313*, 259-266. DOI: 10.1016/j.apsusc.2014.05.201
17. Mabileau, G.; Bourdon, S.; Joly-Guillou, M. L.; Filmon, R.; Baslé, M. F.; Chappard, D. Influence of Fluoride, Hydrogen Peroxide and Lactic Acid on the Corrosion Resistance of Commercially Pure Titanium. *Acta Biomater.* **2006**, *2*, 121-129. DOI: 10.1016/j.actbio.2005.09.004
18. Virtanen, S.; Milosev, I.; Gomez-Barrena, E.; Trebse, R.; Salo, J.; Konttinen, Y. T. Special Modes of Corrosion Under Physiological and Simulated Physiological Conditions. *Acta Biomater.* **2008**, *4*, 468-476. DOI: 10.1016/j.actbio.2007.12.003

19. Gilbert, J. L.; Jacobs, J. J. In *Modularity of Orthopedic Implants*; Marlowe, D. E.; Parr, J. E.; Mayor, M. B., Eds.; American Society Testing and Materials: West Conshohocken, PA, 1997; p 45. DOI: 10.1520/stp12020s
20. Hallam, P.; Haddad, F.; Cobb, J. Pain in the Well-Fixed, Aseptic Titanium Hip Replacement - the Role of Corrosion. *J. Bone Jt. Surg., Br. Vol.* **2004**, *86B*, 27-30. DOI: 10.1302/0301-620x.86b1.14326
21. Gilbert, J. L.; Kubacki, G. W. In *Oxidative Stress and Biomaterials*; Butterfield, D. A., Ed.; Academic Press: London, 2016; p 59. DOI: 10.1016/B978-0-12-803269-5.00003-6
22. Fonseca, C.; Barbosa, M. A. Corrosion Behaviour of Titanium in Biofluids Containing H₂O₂ Studied by Electrochemical Impedance Spectroscopy. *Corros. Sci.* **2001**, *43*, 547-559. DOI: 10.1016/s0010-938x(00)00107-4
23. Tengvall, P.; Lundström, I.; Sjöqvist, L.; Elwing, H.; Bjursten, L. M. Titanium-Hydrogen Peroxide Interaction: Model Studies of the Influence of the Inflammatory Response on Titanium Implants. *Biomaterials* **1989**, *10*, 166-175. DOI: 10.1016/0142-9612(89)90019-7
24. Pan, J.; Thierry, D.; Leygraf, C. Electrochemical and XPS Studies of Titanium for Biomaterial Applications with Respect of the Effect of Hydrogen Peroxide. *J. Biomed. Mater. Res.* **1994**, *28*, 113-122. DOI: 10.1002/jbm.820280115
25. Pan, J.; Thierry, D.; Leygraf, C. Electrochemical Impedance Spectroscopy Study of the Passive Oxide Film on Titanium for Implant Application. *Electrochim. Acta* **1996**, *41*, 1143-1153. DOI:10.1016/0013-4686(95)00465-3

26. Pan, J.; Thierry, D.; Leygraf, C. Hydrogen Peroxide Toward Enhanced Oxide Growth on Titanium in PBS Solution: Blue Coloration and Clinical Relevance. *J. Biomed. Mater. Res.* **1996**, *30*, 393-402. DOI: 10.1002/(sici)1097-4636(199603)30:3<393::aid-jbm14>3.0.co;2-l
27. Mu, Y.; Kobayashi, T.; Sumita, M.; Yamamoto, A.; Hanawa, T. Metal Ion Release from Titanium with Active Oxygen Species Generated by Rat Macrophages In Vitro. *J. Biomed. Mater. Res.* **2000**, *49*, 238-243. DOI: 10.1002/(SICI)1097-4636(200002)49:2<238::AID-JBM12>3.0.CO;2-J
28. Lin, H.-Y.; Bumgardner, J. D. In Vitro Biocorrosion of Ti-6Al-4V Implant Alloy by a Mouse Macrophage Cell Line. *J. Biomed. Mater. Res., Part A* **2004**, *68A*, 717-724. DOI: 10.1002/jbm.a.20092
29. Hiromoto, S.; Hanawa, T. Corrosion of Implant Metals in the Presence of Cells. *Corros. Rev.* **2006**, *24*, 323-351.
30. Mantovani, A.; Sica, A.; Locati, M. Macrophage Polarization Comes of Age. *Immunity* **2005**, *23*, 344-346. DOI: 10.1016/j.immuni.2005.10.001
31. Tan, H.-Y.; Wang, N.; Li, S.; Hong, M.; Wang, X.; Feng, Y. The Reactive Oxygen Species in Macrophage Polarization: Reflecting Its Dual Role in Progression and Treatment of Human Diseases. *Oxid. Med. Cell. Longevity* **2016**, *2016*, 2795090. DOI: 10.1155/2016/2795090
32. Martinez, F. O.; Gordon, S. The M1 and M2 Paradigm of Macrophage Activation: Time for Reassessment. *F1000Prime Rep.* **2014**, *6*, 13. DOI: 10.12703/P6-13

33. Kraaij, M.D.; Koekkoek K.M.; van der Kooij, S.W.; Gelderman, K.A.; van Kooten, C. Subsets of Human Type 2 Macrophages Show Differential Capacity to Produce Reactive Oxygen Species. *Cell. Immunol.* **2013**, *284*, 1-8. DOI: 10.1016/j.cellimm.2013.07.006
34. Genin, M.; Clement, F.; Fattaccioli, A.; Raes, M.; Michiels, C. M1 and M2 Macrophages Derived from THP-1 cells Differentially Modulate the Response of Cancer Cells to Etoposide. *BMC Cancer.* **2015**, *15*, 577. DOI: 10.1186/s12885-015-1546-9
35. Vyas, N.; Sammons, R. L.; Addison, O.; Dehghani, H.; Walmsley, A. D. A Quantitative Method to Measure Biofilm Removal Efficiency from Complex Biomaterial Surfaces Using SEM and Image Analysis. *Sci. Rep.* **2016**, *6*, 32694. DOI: 10.1038/srep32694
36. Arganda-Carreras, I.; Kaynig, V.; Rueden, C.; Eliceiri, K. W.; Schindelin, J.; Cardona, A.; Sebastian Seung, H. Trainable Weka Segmentation: a Machine Learning Tool for Microscopy Pixel Classification. *Bioinformatics* **2017**, *33*, 2424-2426. DOI: 10.1093/bioinformatics/btx180
37. Schindelin, J.; Arganda-Carreras, I.; Frise, E.; Kaynig, V.; Longair, M.; Pietzsch, T.; Preibisch, S.; Rueden, C.; Saalfeld, S.; Schmid, B.; Tinevez, J. Y.; White, D. J.; Hartenstein, V.; Eliceiri, K.; Tomancak, P.; Cardona, A. Fiji: an Open-Source Platform for Biological-Image Analysis. *Nat. Methods* **2012**, *9*, 676-682. DOI: 10.1038/nmeth.2019
38. Blackwood, D. J.; Peter, L. M.; Williams, D. E. Stability and Open Circuit Breakdown of the Passive Oxide Film on Titanium. *Electrochim. Acta* **1988**, *33*, 1143-1149. DOI: 10.1016/0013-4686(88)80206-8

39. Yu, F.; Addison, O.; Davenport, A. J. A Synergistic Effect of Albumin and H₂O₂ Accelerates Corrosion of Ti6Al4V. *Acta Biomater.* **2015**, *26*, 355-365. DOI: 10.1016/j.actbio.2015.07.046
40. Akimoto, T.; Ueno, T.; Tsutsumi, Y.; Doi, H.; Hanawa, T.; Wakabayashi, N., Evaluation of Corrosion Resistance of Implant-Use Ti-Zr Binary Alloys with a Range of Compositions. *J. Biomed. Mater. Res., Part B* **2018**, *106*, 73-79. DOI: 10.1002/jbm.b.33811
41. Fahey, J.; Holmes, D.; Yau, T. L. Evaluation of Localized Corrosion of Zirconium in Acidic Chloride Solutions. *Corrosion* **1997**, *53*, 54-61. DOI: 10.5006/1.3280434
42. Palit, G. C.; Gadiyar, H. S. Pitting Corrosion of Zirconium in Chloride Solution. *Corrosion* **1987**, *43*, 140-148.
43. Mosser, D. M.; Edwards, J. P. Exploring the Full Spectrum of Macrophage Activation. *Nat. Rev. Immunol.* **2008**, *8*, 958-969. DOI: 10.1038/nri2448
44. Dale, D. C.; Boxer, L.; Liles, W. C. The Phagocytes: Neutrophils and Monocytes. *Blood* **2008**, *112*, 935-945. DOI: 10.1182/blood-2007-12-077917
45. Moore, L.B.; Kyriakides, T.R. Molecular Characterization of Macrophage-Biomaterial Interactions. *Adv. Exp. Med. Biol.* **2015**, *865*, 109-122. DOI: 10.1007/978-3-319-18603-0_7.
46. McNally, A.K.; Anderson, J.M. Macrophage Fusion and Multinucleated Giant Cells of Inflammation. *Adv. Exp. Med. Biol.* **2011**, *713*, 97-111. DOI: 10.1007/978-94-007-0763-4_7
47. Sheikh, Z.; Brooks, P.J.; Barzilay, O.; Fine, N.; Glogauer, M. Macrophages, Foreign Body Giant Cells and Their Response to Implantable Biomaterials. *Materials.* **2015**, *28*, 5671-5701 DOI: 10.3390/ma8095269.

48. Moore, L.B.; Sawyer, A.J.; Charokopos, A.; Skokos, E.A.; Kyriakides, T.R. Loss of Monocyte Chemoattractant Protein-1 Alters Macrophage Polarization and Reduces NFκB Activation in the Foreign Body Response. *Acta Biomater.* **2015**, *11*, 37-47. DOI:10.1016/j.actbio.2014.09.022.

49. Murphy, F.A.; Schinwald, A.; Poland, C.A.; Donaldson, K. The Mechanism of Pleural Inflammation by Long Carbon Nanotubes: Interaction of Long Fibres with Macrophages Stimulates Them to Amplify Pro-inflammatory Responses in Mesothelial Cells. *Part. Fibre. Toxicol.* **2012**, *9*, 8. DOI: 10.1186/1743-8977-9-8.

50. Liu, X.; Ramsey, M. M.; Chen, X.; Koley, D.; Whiteley, M.; Bard, A. J. Real-Time Mapping of a Hydrogen Peroxide Concentration Profile Across a Polymicrobial Bacterial Biofilm Using Scanning Electrochemical Microscopy. *Proc. Natl. Acad. Sci. U. S. A.* **2011**, *108*, 2668-2673. DOI: 10.1073/pnas.1018391108

FOR TABLE OF CONTENTS ONLY

